

LSTM-Based ECG Classification for Continuous Monitoring on Personal Wearable Devices

Saeed Saadatnejad, Mohammadhosein Oveisi, and Matin Hashemi

Abstract—A novel ECG classification algorithm is proposed for continuous cardiac monitoring on wearable devices with limited processing capacity. The proposed solution employs a novel architecture consisting of wavelet transform and multiple LSTM recurrent neural networks (Fig. 1). Experimental evaluations show superior ECG classification performance compared to previous works. Measurements on different hardware platforms show the proposed algorithm meets timing requirements for continuous and real-time execution on wearable devices. In contrast to many compute-intensive deep-learning based approaches, the proposed algorithm is lightweight, and therefore, brings continuous monitoring with accurate LSTM-based ECG classification to wearable devices. The source code is available online [1].

Index Terms—Continuous cardiac monitoring, Electrocardiogram (ECG) classification, Deep learning, Long Short-Term Memory (LSTM), Wearable devices

I. INTRODUCTION

CARDIOVASCULAR diseases (CVDs) such as myocardial infarction, cardiomyopathy and myocarditis are the leading causes of death in the world. An estimated 17.7 million people died from CVDs in 2015, representing 31% of all global deaths reported by the World Health Organization [2]. Cardiac arrhythmias are among the most important CVDs.

Electrocardiogram (ECG) signal represents electrical activities of the heart and is widely used in detection and classification of cardiac arrhythmias. A trained cardiologist can detect arrhythmias by visually inspecting the ECG waveform. However, arrhythmias occur intermittently, especially in early stages of the problem. Hence, it is difficult to detect them in a short time window of the ECG waveform. Therefore, continuous monitoring of patients' heartbeats in daily life is crucial to arrhythmia detection [3], [4].

Wearable devices provide a platform for this purpose [4]. Our approach is to locally execute the ECG classification algorithm on patients' personal wearable devices. Local execution allows for continuous operation regardless of the network speed and availability. In addition, it allows data to stay on the wearable device and hence avoids privacy issues of cloud-assisted processing. Our approach is different from offline processing of stored ECG signals, or remote processing on powerful cloud servers [5], [6].

Continuous monitoring on wearable devices require the automated ECG classification algorithm to be both *accurate* and *light-weight* at the same time. This forms our main focus

in this work. Note that wearable devices have small and low-power processors which are much slower compared to desktop and server processors.

Many previous algorithms are based on morphological features and classical signal processing techniques [7]–[18]. Since the ECG waveform and its morphological characteristics, such as the shapes of QRS complex and P waves, significantly vary under different circumstances and for different patients, the fixed features employed in such algorithms are not sufficient for accurately distinguishing among different types of arrhythmia for all patients [19], [20].

To extract the features automatically and increase the heart-beat classification accuracy, deep-learning based algorithms including deep convolutional neural networks and recurrent neural networks have recently been proposed [20]–[23].

This paper proposes a novel ECG classification algorithm based on LSTM recurrent neural networks (RNNs). See Fig. 1. The proposed algorithm employs RNNs because the ECG waveform is naturally fit to be processed by this type of neural network. The reason lies within the electrical conduction system of the heart. See Fig. 2. The sinoatrial node generates a pacemaker signal which travels through internodal pathways to the atrioventricular node. The conduction slows through the atrioventricular node which causes a time delay. Next, the signal travels through the bundle of His to the heart apex and the Purkinje fibers, then finally to the ventricles [24]. The above sequence of electrical activities are reflected into the ECG waveform (Fig. 2), and therefore, temporal dependencies naturally exist in this waveform. RNNs capture such temporal dependencies in sequential data more efficiently compared to other types of neural networks.

As shown in Fig. 1, the proposed algorithm employs both LSTM recurrent neural networks and classical features, i.e., wavelet, at the same time. The additional features help to better capture the patterns in the ECG waveform. In addition, the proposed algorithm merges the arrhythmia predictions from small LSTM models as opposed to constructing one large model. The total computational costs of multiple smaller LSTM models is lower than one larger model.

As a result, in contrast to many previous deep-learning based approaches which are computationally intensive [21]–[23], the proposed algorithm increases the classification accuracy without significantly increasing the computational costs. Hence, it brings continuous monitoring with accurate LSTM-based ECG classification to personal wearable devices.

Experimental results show effectiveness of the proposed solution. Reporting the accuracy of ECG classification algorithms has been standardized by the Association for the

Authors are with the Learning and Intelligent Systems Laboratory, Department of Electrical Engineering, Sharif University of Technology. Webpage: <http://lis.ee.sharif.edu>, E-mail: saeedsa@ee.sharif.edu, oveisi@ee.sharif.edu, matin@sharif.edu (corresponding author).

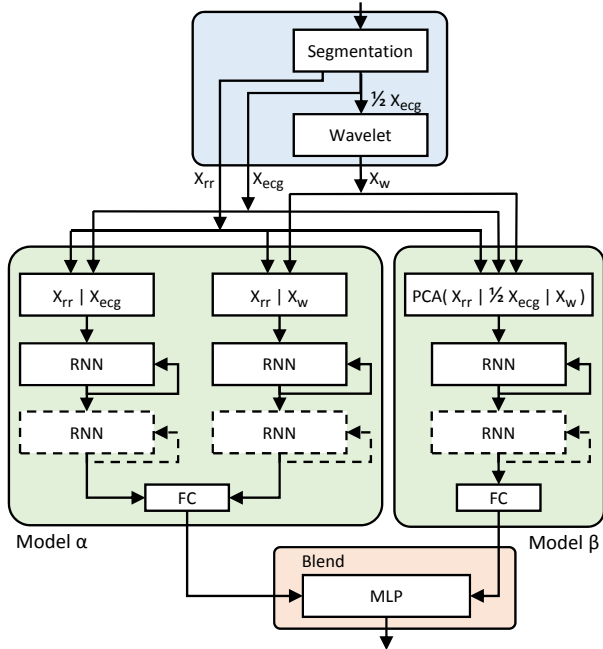


Fig. 1: Overall view of the proposed algorithm.

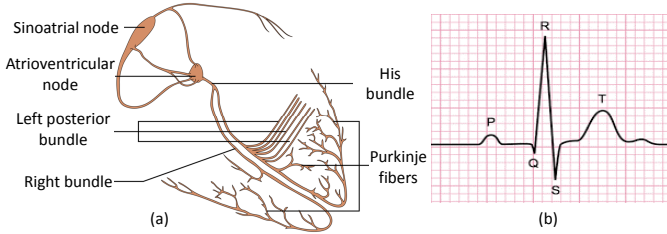


Fig. 2: (a) Electrical conduction system of the heart, and (b) the ECG waveform [24], [42].

Advancement of Medical Instrumentation (AAMI) [25]. Our proposed algorithm is evaluated using the same ECG signals that were employed in the previous works that conform to this standard. Experimental evaluations demonstrate that the proposed algorithm has superior classification performance compared to such methods. For instance, F_1 score is 3.3% and 15.5% higher in classifying ventricular ectopic beats (VEB) from non-VEBs and supraventricular ectopic beats (SVEB) from non-SVEBs, respectively. Note that SVEB detection is considered to be more difficult than VEB detection.

Computational requirements of the proposed algorithm is evaluated as well. Empirical measurements on small and low-power hardware platforms show that the proposed algorithm meets timing requirements for continuous and real-time execution on such platforms.

Previous works have lower classification performance [8]–[20], are not suitable for continuous execution on wearable devices due to high computational intensity [21]–[23], do not include all the standard AAMI classes [26]–[31], or focus on other problems related to processing of ECG signals [32]–[41].

Detailed comparisons with all the related works are presented in Section II. The proposed algorithm and its training procedure are discussed in Sections III and IV. The experiment results are discussed in Section V. Concluding remarks are presented in Section VI.

II. RELATED WORKS

Many previous ECG classification algorithms are mainly focused on signal processing techniques including extraction of morphological features [8], frequency domain analysis [9], Hermite function decomposition [10], wavelet transform [11], [12], support vector machines [13] and hidden Markov models [14]. Hu et. al [15] proposed a mixture of experts method for patient-adaptable heartbeat classification. Chazal and Reilly [16] proposed a personalized heartbeat classification algorithm based on linear discriminant analysis on ECG morphology and timing interval features. Jiang and Kong [17] proposed a block-based neural network algorithm, and Ince et. al. [18] proposed particle swarm optimization for artificial neural networks, both for patient-specific heartbeat classification. Compared to the above solutions, the proposed algorithm achieves higher classification performance. See Section V.

Recent approaches have focused on deep learning. Kiranyaz et. al. [20] proposed a one-dimensional convolutional neural network algorithm. Both the above and the proposed methods meet timing requirements, but our proposed method achieves higher classification performance, especially in SVEB detection. In [20], a heartbeat trio is fed into the convolutional neural network in order to capture the effect of nearby heartbeats in classifying the current heartbeat. This overhead is not necessary in our method because the LSTM cells capture temporal dependencies automatically and more efficiently. In addition, our proposed solution combines the arrhythmia predictions from small LSTM models as opposed to constructing one large model.

Rajpurkar et. al. [21] proposed a much deeper CNN. This computationally intensive algorithm consists of 34 layers and is not suitable for execution on wearable devices due to its very long execution time. Jun et. al. [22] proposed another CNN algorithm with 11 layers but their convolutions are two-dimensional and hence much more computationally intensive than one-dimensional convolutions. In contrast, our proposed method is designed from ground up to be lightweight, and hence, meets timing requirements for continuous execution on wearable devices with limited processing capacity.

A general regression neural network model was proposed in [23] for classification of long-term ECG signals. This algorithm is designed for offline processing and requires the entire recorded data. The algorithm is accelerated on high-performance GPUs in order to reduce the execution time. Teijeiro et. al. [7] proposed an ECG clustering algorithm that requires the entire recorded data. As opposed to offline solutions which work on recorded data, the proposed algorithm in this paper is able to process real-time ECG signals.

There are many other deep-learning based ECG classification methods in the literature that do not comply with AAMI standards and hence are not directly comparable with the proposed solution. For instance, many only consider a selected subset of the standard classes [26]–[31], which makes the design and training of neural networks much simpler because not all the challenging cases are included. The proposed solution fully complies with AAMI standards [25], the results are reported based on the standard and openly available MIT-

BIH dataset [43] and all standard classification metrics have been calculated and reported.

Deep learning has also been applied to other problems related to analysis of ECG signals, for instance, ECG-based biometrics [32], [33], detecting atrial fibrillation (AF) [34]–[40] and diagnosis based on hospital records [41].

III. PROPOSED ALGORITHM

Fig. 1 presents an overall view of the proposed algorithm. First, the incoming digitized ECG samples are segmented into heartbeats and their RR interval and wavelet features are extracted (Sections III-A and III-B). Next, the ECG signal along with the extracted features are fed into two RNN-based models which classify every heartbeat (Sections III-C and III-D). The two outputs are then blended to form the final classification for every heartbeat (Section III-E). The details are discussed in the following. The training procedure is discussed later in Section IV.

A. Segmentation and RR Intervals

The digitized ECG samples are segmented into a sequence of heartbeats. The segmentation is performed based on detecting the R peaks. In specific, every segment (heartbeat) contains 0.25 seconds of the input ECG signal before the detected R peak and 0.45 seconds after.

R peak detection algorithms are well established and highly accurate [44], [45]. In our segmentation process, Pan-Tompkin's algorithm [44] is used. As part of Pan-Tompkin's algorithm, the time intervals between consecutive R peaks are calculated as well. Let RR_i denote the time interval from R peak $i - 1$ to R peak i . Based on this information, we also extract the following features for heartbeat i : I) RR_i as the past interval, II) RR_{i+1} as the next interval, III) $\frac{1}{10} \sum_{k=i-4}^{i+5} RR_k$ as the local average of the five past and the five next intervals, and IV) the average RR in each person's train data.

Note that features II and III require access to future heartbeats. However, as opposed to processing previously stored ECG signals, future information is not available in our setting. This is because the proposed algorithm is designed for continuous monitoring. We mitigate this problem by buffering the ECG signal in a first-in-first-out (FIFO) memory in real-time. This buffer is implemented in software and must be small. By always classifying the heartbeat which falls in the middle of this buffer, access to the near past and the near future information is made possible.

The fourth feature is the average RR in each person's train data. Section IV-A discusses the train data. This feature varies among people with different average heart rates. For example, it is larger in athletes because they have slower heart rates.

Besides the above RR features which are accurately extracted with minimal computations, the proposed algorithm does not employ other hand-crafted morphological features such as those that are based on Q , S or T . This is because such features are not optimal in representing the characteristics of the underlying signal. In addition, they are fixed for all patients under all circumstances and therefore do not efficiently represent the differences among the arrhythmia classes [19],

[20]. Instead, we let the features be automatically extracted using wavelet and recurrent neural networks as discussed in the following sections.

B. Wavelet Features

ECG signal has non-stationary characteristics. Therefore, to capture both the time and the frequency domain information, discrete wavelet transform [46] is applied to the digitized ECG samples in every heartbeat.

In specific, Daubechies wavelet family is selected because of its similarity with the ECG signal. Low-order Daubechies wavelets have high time resolution but poor frequency resolution, whereas high-order ones have high frequency resolution and poor time resolution. Daubechies type 2, i.e., db2, is employed in the proposed algorithm.

Total length of the wavelet coefficients for every heartbeat, i.e., $|X_w|$, is determined based on the wavelet type and decomposition level, as well as, its input length. The wavelet input, i.e., X_{ecg} in Fig 1, is down sampled by a factor of 2 before applying the wavelet transform. This cuts the length of the wavelet coefficients to about half, and thus, helps to reduce the computation time of the following steps.

C. RNN-based Models

For every heartbeat, the input ECG samples (X_{ecg}) along with the extracted RR intervals and wavelet features (X_{rr} and X_w) are provided to two separate RNN-based models, called model α and model β . See Fig. 1. The two models make separate arrhythmia predictions which are then blended to form the final prediction for every heartbeat.

Employing X_{rr} and X_w in addition to X_{ecg} helps the RNN models capture patterns in the ECG signals more efficiently. The additional features provide processed information to the RNN models. Therefore, accurate results can be reached with smaller and hence faster RNNs. Employing multiple smaller RNNs in parallel instead of one larger RNN helps to increase the accuracy without significantly increasing the computational costs. See (10).

In model α , first X_w and X_{ecg} are processed separately and then the outputs are combined. In model β , however, X_w and X_{ecg} are first combined and then processed. The details are discussed as follows.

Model α : As shown in Fig. 1, model α consists of two branches. Every branch includes one or two RNNs. Every RNN includes a number of hidden units. The internal functionality of the RNN cells are discussed in Section III-D.

The input to the left branch is denoted by $X^{\alpha 1}$ and is formed by concatenating X_{rr} and X_{ecg} . The RNN cells in this branch process the array $X^{\alpha 1}$ and extract $N_h^{\alpha 1}$ features. Similarly, the right branch concatenates X_{rr} and X_w into array $X^{\alpha 2}$, then, processes this array and extracts $N_h^{\alpha 2}$ features.

The features that are extracted by the two branches in model α are concatenated and fed into a fully connected neural network layer in order to produce the probability of all the N_y output arrhythmia classes. The output classes are discussed later in Section V. The dimension of this fully connected

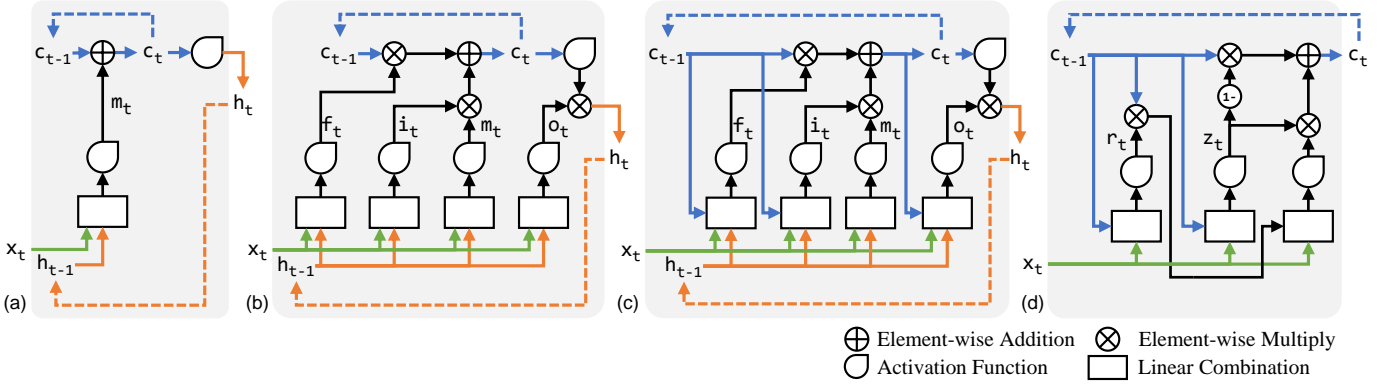


Fig. 3: (a) Simple RNN Cell, (b) Long Short-Term Memory (LSTM), (c) LSTM with Peepholes, (d) Gated Recurrent Unit (GRU).

layer is therefore equal to $(N_h^{\alpha+1} + N_h^{\alpha+2}) \times N_y$. The maximum probability determines the arrhythmia class that is predicted by model α .

Model β : This model consists of only one branch. See Fig. 1. As opposed to processing X_{ecg} and X_w in two separate RNN branches and then combining the outputs, here the inputs are combined. In specific, array X^β is formed by concatenating a down sampled version of X_{ecg} with X_{rr} and X_w , followed by applying PCA on the concatenated array. X^β is then processed by the RNNs in this model and N_h^β features are extracted. The features are fed into a fully connected neural network layer with dimension $N_h^\beta \times N_y$. The output is the probability of all the N_y output arrhythmia classes.

Models α and β include a number of hyper-parameters, namely, the number of RNNs in every branch, the number of hidden units in every RNN, and the RNN cell types. The hyper-parameters are determined later in Section IV-D.

D. RNN Cells

Internal functionality of different RNN cell types is described below. Classification performance of the proposed algorithm is evaluated with the following cell types in Section V.

Simple RNN Cell: Fig. 3(a) shows a simple RNN cell. x_t is the input vector at time t . h_t and c_t are state vectors which are carried from time $t-1$ to time t , and therefore, act as memory by encoding previous information. h_t is also considered as the cell output at time t . Size of vectors h and c is denoted by N_h and is known as the number of hidden units. The cell works based on the following equations.

$$m_t[j] = \tanh \left(\sum_{k \in [1, N_x]} w[j, k] x_t[k] + \sum_{k \in [1, N_h]} u[j, k] h_{t-1}[k] + b[j] \right) \quad (1)$$

$$c_t[j] = c_{t-1}[j] + m_t[j] \quad (2)$$

$$h_t[j] = \tanh(c_t[j]) \quad (3)$$

As shown in (1), an intermediate vector m_t is formed by applying \tanh activation function on a linear combination of x_t and h_{t-1} , i.e., current input and previous output, respectively. $j \in [1, N_h]$. Weight matrices w and u as well as the bias

vector b are constants that will be determined in the training phase (Section IV).

The internal state vector, i.e., c_t , is formed by accumulating m_t over time. See (2). The output vector h_t is formed by applying \tanh activation function on c_t . See (3). It can be seen that the output is related to all previous inputs.

Long Short-Term Memory (LSTM): In the above simple RNN cell the effect of all previous information is accumulated in the internal state vectors. This may lead to vanishing or exploding gradients during gradient descent training. Gradient-based algorithms fail when temporal dependencies get too long. This is because gradient values can increase or decrease exponentially [47].

LSTM solves this issue by allowing to forget according to the actual dependencies which exist in the problem. The dependencies are automatically extracted based on the data. This is achieved through forget, input and output gates [47]. See Fig. 3(b). The gate signals are produced based on current input, i.e., x_t , and previous output, i.e., h_{t-1} , as shown in (4), (5) and (6).

$$f_t[j] = \sigma \left(\sum_{k \in [1, N_x]} w_f[j, k] x_t[k] + \sum_{k \in [1, N_h]} u_f[j, k] h_{t-1}[k] + b_f[j] \right) \quad (4)$$

$$i_t[j] = \sigma \left(\sum_{k \in [1, N_x]} w_i[j, k] x_t[k] + \sum_{k \in [1, N_h]} u_i[j, k] h_{t-1}[k] + b_i[j] \right) \quad (5)$$

$$o_t[j] = \sigma \left(\sum_{k \in [1, N_x]} w_o[j, k] x_t[k] + \sum_{k \in [1, N_h]} u_o[j, k] h_{t-1}[k] + b_o[j] \right) \quad (6)$$

In the above equations, σ denotes the *sigmoid* activation function, $j \in [1, N_h]$, and weight matrices w and u as well as the bias vector b are constants that will be determined in the training phase.

In the LSTM cell, m_t is computed as before, i.e., as in (1), but (2) and (3) are modified based on the forget, input and output gate signals as the following.

$$c_t[j] = f_t[j] \times c_{t-1}[j] \quad (7)$$

$$+ i_t[j] \times m_t[j]$$

$$h_t[j] = o_t[j] \times \tanh(c_t[j]) \quad (8)$$

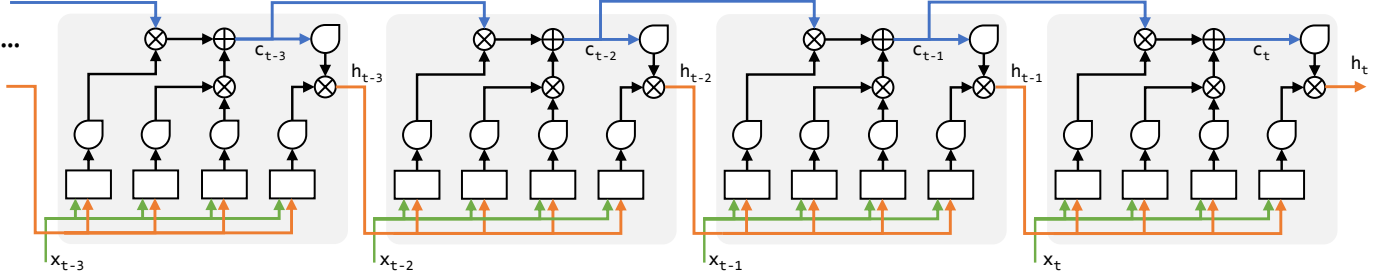


Fig. 4: Unfolded view of the LSTM recurrent neural network.

As shown in (7), the forget gate f_t controls carrying of state vector c from time $t - 1$ to time t . The input gate i_t adjusts the accumulation of m_t in c_t . As shown in (8), the output h_t is formed by applying \tanh activation function on c_t , and is then adjusted by the output gate o_t .

Note that the LSTM output still depends on all previous inputs. To make this point more clear, Fig. 4 shows an unfolded view of the LSTM recurrent neural network in time. The three gates do not completely discard but only control accumulation of previous information over time.

LSTM with Peepholes: The LSTM cell can be extended by adding extra connections from the internal state vector to the forget, input and output gates. The extra connections are marked with blue color in Fig. 3(c). The gate signals are formed based on a linear combination of x_t , h_{t-1} and now also c_{t-1} [48]. Detailed equations are omitted for brevity.

Gated Recurrent Unit (GRU): This cell is a simplified version of the LSTM cell which merges the two state vectors into one and also employs a different gating strategy [49]. See Fig. 3(d). The cell works based on the following equation.

$$c_t[j] = (1 - z_t[j]) \times c_{t-1}[j] + z_t[j] \times \tanh\left(\sum_{k \in [1, N_x]} w[j, k] x_t[k] + \sum_{k \in [1, N_h]} u[j, k] r_t[k] c_{t-1}[k] + b[j]\right) \quad (9)$$

In the above equation, z_t and r_t are update and reset gate signals, respectively, and are formed similar to the LSTM gate signals as linear combinations of x_t and c_{t-1} .

Complexity Analysis: The above RNN cells perform several matrix and vector operations. For instance, the LSTM cell requires four matrix vector multiplications of size $N_h \times N_x$, four matrix vector multiplications of size $N_h \times N_h$ and several vector operations of size N_h . Total computational complexity for every execution of an RNN cell is therefore equal to

$$aN_x N_h + bN_h^2 + cN_h + d \quad (10)$$

where a , b , c and d depend on the cell type. The computational complexity has a quadratic growth with respect to the number of hidden units, i.e., N_h . Therefore, multiple smaller RNNs have lower computational costs in total compared to one larger RNN.

E. Blend Model

Ensemble methods such as blending are designed to boost the classification accuracy by blending the predictions made by multiple learning models [50], [51].

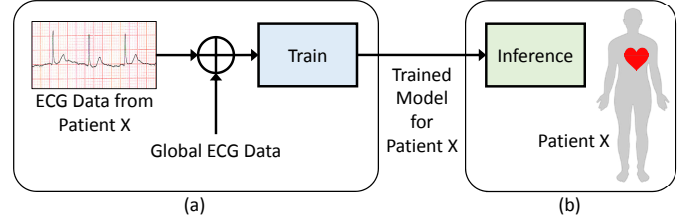


Fig. 5: (a) Patient-specific training. (b) Continuous ECG monitoring and heartbeat classification in real-time.

Only two models are blended in our proposed algorithm in order to keep the computational requirement as low as possible. See Fig. 1. For every heartbeat, first, the two RNN-based models α and β independently compute the probability of all the N_y output arrhythmia classes. Then the two results are blended to form the final probability of the N_y output classes.

The blend model is implemented using a multi-level perceptron (MLP). The input and output layers have $2 \times N_y$ and N_y neurons, respectively.

IV. TRAINING PROCEDURE

A. Patient-Specific Training

We employ a patient-specific training procedure. In other words, the model is trained for every patient individually [15]–[18], [20]. Once the model is trained for a patient, continuous ECG monitoring and heartbeat classification is performed in real-time based on the trained model. See Fig. 5.

The training data is composed of two parts, patient-specific ECG data and global ECG data. The first part is specific to every patient and is helpful in increasing the classification accuracy due to existing similarities among the heartbeats of every patient. According to AAMI standards [25], this ECG data can be at most five minutes long. Global data is the same for all patients. It consists of a small number of representative heartbeats from all arrhythmia classes. It helps the model learn other arrhythmia patterns that are not included in the patient-specific data. Details of the ECG signals employed in our experiments are presented in Section V.

B. Train the RNN Models

Back propagation (BP) is a well known method for training feed-forward neural networks such as convolutional neural networks (CNNs). This method cannot be applied to RNNs because of the existing temporal dependencies in the model,

i.e., the feedback loops in Fig. 3 which carry previous information through time.

To train RNN models, train data is split into batches of several heartbeats each. The heartbeats are processed one after another as discussed in the following. The model weights are updated upon completion of every batch.

In the beginning of every batch, vector h is set to zero and vector c is set randomly. Then the input data is forward-propagated over the network, and error is calculated until the batch finishes. Next, the error is back-propagated over the unfolded network in time, the weight matrices change in all instances and their mean is set as the updated weight. This method is known as back propagation through time (BPTT) [52].

The above procedure continues until all batches are processed. The optimization method employed in our work is adaptive moment estimation algorithm, a.k.a., Adam [53].

C. Train the Blend Model

First, the two RNN-based models, i.e., model α and model β , are trained independently as discussed above. Next, their output arrhythmia predictions for the heartbeats in the train data are used to train the blend model, i.e., the multi-level perceptron in Fig. 1. The training is performed using back propagation (BP).

D. Hyper-Parameter Selection

Learning algorithms related to neural networks often involve hyper-parameters. There are a number of guidelines and recommendations for selecting the hyper-parameters [54]. The procedures discussed below are performed on the cross validation set in order to avoid over-fitting.

For the RNN-based models α and β , we perform a grid search for the number of recurrent layers, i.e., the number of RNNs in every branch, and also, the number of hidden units, i.e., $N_h^{\alpha 1}$, $N_h^{\alpha 2}$ and N_h^{β} . For the cell type in the RNN-based models, we consider simple RNN cell, LSTM, LSTM with peephole, and GRU. We found that RNN models with the LSTM cell achieve consistently strong results.

V. EXPERIMENTS

A. Setup and ECG Data

The proposed algorithm is implemented in the Python language and TensorFlow library. Our source code is available online [1]. TensorFlow is a machine learning library that works based on dataflow graphs. Here the graph nodes perform the required computations and the graph edges transfer multidimensional arrays (tensors) between the nodes.

MIT-BIH ECG arrhythmia database [43] is used to evaluate the proposed algorithm and compare its performance with previous works. This database consists of ECG recordings of 48 patients. Each record has two leads. The first lead is modified limb lead II (MLII). The second lead is modified lead V1 or in some cases V2, V4 or V5. Two or more cardiologists independently annotated each record.

The database contains two sets of data, which we call DS100 and DS200. DS100 (numbered from 100 to 124 with some numbers missing) includes representative samples of the variety of ECG waveforms and artifacts that an arrhythmia detector might encounter in routine clinical practice. DS200 (numbered from 200 to 234 with some numbers missing) includes complex ventricular, junctional, and supraventricular arrhythmias and conduction abnormalities. According to AAMI standards, the records which contain paced beats, i.e. records 102, 104, 107, and 217, are excluded from the study [25].

Global training data is formed by randomly selecting representative heartbeats from all arrhythmia classes in DS100 records. Patient-specific training data is the first five minutes of a patient's record in DS200. This is in compliance with AAMI standards [25]. Test data is all the records in DS200. The first five minutes of all the records are skipped in the test data.

B. Classification Performance

In our experimental evaluations, every heartbeat is classified into the seven arrhythmia classes that are shown in Table I. Based on AAMI standards [25], many previous works employ five class labels, namely, N, S, V, F and Q [17], [18], [20]. However, to have more resolution, we split class N into three classes by separating two conduction abnormalities known as left bundle branch block (L) and right bundle branch block (R). As shown in Table II(a), the proposed algorithm is able to distinguish L and R from N very efficiently.

When comparing the proposed algorithm with previous works, L and R labels are merged back into N. See Table II(b). In order to report performance results for binary classification of ventricular ectopic beats (VEB) from non-VEBs and also supraventricular ectopic beats (SVEB) from non-SVEBs, the following statistical metrics are extracted from the confusion matrix. Accuracy is defined as the number of correct predictions divided by the total number of predictions.

$$Acc = \frac{TP+TN}{TP+TN+FP+FN} \quad (11)$$

The terms TP, TN, FP and FN denote true positive, true negative, false positive and false negative in the binary classification, respectively. Sensitivity is defined as the number of correct positive predictions divided by the total number of positive events.

$$Sen = \frac{TP}{TP+FN} \quad (12)$$

Specificity is defined as the number of correct negative predictions divided by the total number of negative events.

$$Spe = \frac{TN}{TN+FP} \quad (13)$$

Positive predictivity is defined as the number of correct positive predictions divided by all positive predictions.

$$Ppr = \frac{TP}{TP+FP} \quad (14)$$

Since, increasing positive predictivity (Ppr) often decreases sensitivity (Sen) and vice versa, F_1 score is also calculated

| 5 Labels | 7 Labels | Heartbeat types |
|----------|----------|--|
| N | N | Normal beat, atrial escape beat, junctional escape beat |
| | L | Left bundle branch block beat |
| | R | Right bundle branch block beat |
| S | S | Atrial premature beat, aberrated atrial premature beat, junctional premature beat, supraventricular premature beat |
| V | V | Premature ventricular contraction, ventricular escape beat |
| F | F | Fusion of ventricular and normal beat |
| Q | Q | Paced beat, fusion of paced and normal beat, unclassifiable beat |

TABLE I: Heartbeat classes.

| | | | | | | | | | |
|-----|-----------|---|-------|------|------|------|------|-----|---|
| (a) | Reference | N | L | R | S | V | F | Q | |
| | | N | 35950 | 0 | 5 | 23 | 18 | 44 | 0 |
| | | L | 5 | 3034 | 1 | 0 | 0 | 0 | 0 |
| | | R | 0 | 0 | 2783 | 1 | 0 | 0 | 0 |
| | | S | 672 | 81 | 1 | 1566 | 17 | 3 | 0 |
| | | V | 216 | 1 | 17 | 45 | 4470 | 59 | 0 |
| | | F | 33 | 0 | 0 | 1 | 46 | 532 | 0 |
| | | Q | 6 | 1 | 0 | 0 | 0 | 1 | 0 |

| | | | | | | | |
|-----|-----------|---|-------|------|------|-----|---|
| (b) | Reference | N | S | V | F | Q | |
| | | N | 41778 | 24 | 18 | 44 | 0 |
| | | S | 754 | 1566 | 17 | 3 | 0 |
| | | V | 234 | 45 | 4470 | 59 | 0 |
| | | F | 33 | 1 | 46 | 532 | 0 |
| | | Q | 7 | 0 | 0 | 1 | 0 |

TABLE II: Confusion matrix with (a) 7 and (b) 5 heartbeat classes.

| | | VEB | | | | | | SVEB | | | | | |
|-----------|----------------------|------|------|------|------|------|------|------|------|------|------|------|------|
| | | Acc | Sen | Spe | Ppr | F1 | G | Acc | Sen | Spe | Ppr | F1 | G |
| Dataset A | Hu et al. [15] | 94.8 | 78.9 | 96.8 | 75.8 | 77.3 | 77.3 | N/A | N/A | N/A | N/A | N/A | N/A |
| | Proposed | 99.3 | 96.0 | 99.8 | 98.3 | 97.1 | 97.1 | 98.6 | 75.2 | 99.9 | 99.8 | 85.8 | 86.6 |
| Dataset B | Chazal et al. [16] | 99.4 | 94.3 | 99.7 | 96.2 | 95.2 | 95.2 | 95.9 | 87.7 | 96.2 | 47.0 | 61.2 | 64.2 |
| | Proposed | 99.6 | 95.8 | 99.9 | 97.8 | 96.8 | 96.8 | 99.0 | 75.6 | 99.9 | 98.9 | 85.7 | 86.5 |
| Dataset C | Jiang and Kong [17] | 98.1 | 86.6 | 99.3 | 93.3 | 89.8 | 89.9 | 96.6 | 50.6 | 98.8 | 67.9 | 58.0 | 58.6 |
| | Ince et al. [18] | 97.6 | 83.4 | 98.1 | 87.4 | 85.4 | 85.4 | 96.1 | 62.1 | 98.5 | 56.7 | 59.3 | 59.3 |
| | Kiranyaz et al. [20] | 98.6 | 95.0 | 98.1 | 89.5 | 92.2 | 92.2 | 96.4 | 64.6 | 98.6 | 62.1 | 63.3 | 63.3 |
| | Proposed | 99.2 | 93.0 | 99.8 | 98.2 | 95.5 | 95.5 | 98.3 | 66.9 | 99.8 | 95.7 | 78.8 | 80.0 |

TABLE III: Comparing the proposed algorithm with previous works in binary classification of VEB and binary classification of SVEB. Dataset A for VEB classification is 200, 202, 210, 213, 214, 219, 221, 228, 231, 233 and 234. Dataset A for SVEB classification is the same records for VEB classification plus 212, 222 and 232 [15]. Dataset B is 100, 103, 105, 111, 113, 117, 121, 123, 200, 202, 210, 212, 213, 214, 219, 221, 222, 228, 231, 232, 233 and 234 [16]. Dataset C is 200, 201, 202, 203, 205, 207, 208, 209, 210, 212, 213, 214, 215, 219, 220, 221, 222, 223, 228, 230, 231, 232, 233 and 234 [17], [18], [20].

which combines Sen and Ppr into one metric. G score is also calculated for the same purpose.

$$F_1 = \frac{2}{\frac{1}{Sen} + \frac{1}{Ppr}} \quad (15)$$

$$G = \sqrt{Sen \times Ppr} \quad (16)$$

Table III compares the proposed algorithm with previous works. In order to provide thorough and fair comparisons, the proposed algorithm is evaluated based on the exact same data as the previous works. The proposed algorithm cannot be directly compared with other methods that do not comply with AAMI standards or do not employ the openly available MIT-BIH database. To compare the proposed algorithm with the methods in [15] and [16] we consider dataset A and dataset B, respectively. The main dataset which is also employed in [17], [18] and [20] is dataset C. See Table III.

In both VEB and SVEB, the proposed algorithm achieves superior classification performance compared to previous works. In VEB detection, for instance, accuracy is always higher than 99%. It is 4.5%, 0.2% and 0.6% higher than the previous works in datasets A, B and C, respectively. F_1 score is much higher. It is 19.8%, 1.6% and 3.3% higher than the previous works in datasets A, B and C, respectively.

In SVEB detection, accuracy is 3.1% and 1.7% higher than the previous works in datasets B and C, respectively. F_1 score is 24.5% and 15.5% higher than the previous works in datasets B and C, respectively. Note that F_1 score is a more meaningful metric compared to accuracy.

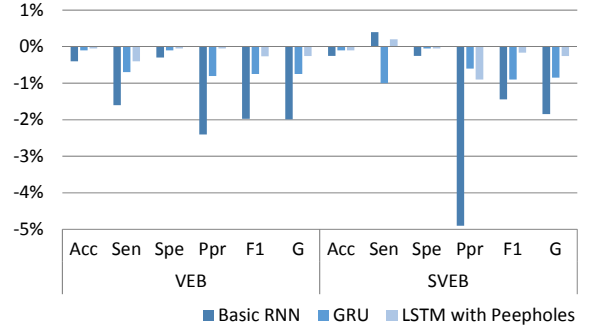


Fig. 6: Degradation of classification performance with different RNN cell types compared to the selected LSTM cell.

C. RNN Cell Types

Fig. 6 compares the effect of using different RNN cell types in the proposed algorithm. In specific, it shows degradation of classification performance as a result of using the simple RNN, GRU and Peephole cells compared with the selected LSTM cell. The Peephole cell is very close to the selected LSTM cell. We employ LSTM because it gives the highest performance, and does not have the extra computations required in the Peephole cell, i.e., the extra blue connections in Fig. 3(c).

D. Execution Time

Personal wearable devices have small and low-power processors which are much slower compared to desktop and server processors. Therefore, to meet timing requirements for

continuous execution, the proposed heartbeat classification algorithm needs to have low computational intensity.

To experimentally evaluate the execution time, we have implemented the inference (test) phase of the proposed algorithm on small and low-power platforms, namely, ARM Cortex A7 and ARM Cortex A53, and measured the execution time. This experiment shows that the proposed algorithm takes about 30 milliseconds to process every heartbeat and hence meets timing requirements for continuous ECG classification.

VI. CONCLUSION

In this paper a novel LSTM-based ECG classification algorithm was proposed which achieves superior classification performance compared to the previous works. In addition, as opposed to many previous deep-learning based algorithms, it has low computational costs and meets timing requirements for continuous execution on wearable devices with limited processing power.

REFERENCES

- [1] The source code will be available online upon final publication of the paper.
- [2] "Cardiovascular diseases (CVDs)," May 2017. [Online]. Available: <http://www.who.int/mediacentre/factsheets/fs317/en/>
- [3] X. Chen, J. Ji, K. Loparo, and P. Li, "Real-time personalized cardiac arrhythmia detection and diagnosis: A cloud computing architecture," in *IEEE EMBS International Conference on Biomedical Health Informatics (BHI)*, Feb 2017, pp. 201–204.
- [4] J. M. Bote, J. Recas, F. Rincn, D. Atienza, and R. Hermida, "A modular low-complexity ecg delineation algorithm for real-time embedded systems," *IEEE Journal of Biomedical and Health Informatics*, vol. 22, no. 2, pp. 429–441, March 2018.
- [5] X. Wang *et al.*, "Enabling smart personalized healthcare: A hybrid mobile-cloud approach for ecg telemonitoring," *IEEE Journal of Biomedical and Health Informatics*, vol. 18, no. 3, pp. 739–745, May 2014.
- [6] J. M. Lillo-Castellano *et al.*, "Symmetrical compression distance for arrhythmia discrimination in cloud-based big-data services," *IEEE Journal of Biomedical and Health Informatics*, vol. 19, no. 4, pp. 1253–1263, July 2015.
- [7] T. Teijeiro, P. Flix, J. Presedo, and D. Castro, "Heartbeat classification using abstract features from the abductive interpretation of the ecg," *IEEE Journal of Biomedical and Health Informatics*, vol. 22, no. 2, pp. 409–420, March 2018.
- [8] P. de Chazal, M. ODwyer, and R. B. Reilly, "Automatic classification of heartbeats using ecg morphology and heartbeat interval features," *IEEE Transactions on Biomedical Engineering*, vol. 51, no. 7, pp. 1196–1206, July 2004.
- [9] K. Minami, H. Nakajima, and T. Toyoshima, "Real-time discrimination of ventricular tachyarrhythmia with fourier-transform neural network," *IEEE Transactions on Biomedical Engineering*, vol. 46, no. 2, p. 179185, Feb. 1999.
- [10] M. Lagerholm, C. Peterson, G. Braccini, L. Edenbrandt, and L. Sornmo, "Clustering ecg complexes using hermite functions and self-organizing maps," *IEEE Transactions on Biomedical Engineering*, vol. 47, no. 7, pp. 838–848, 2000.
- [11] L.-Y. Shyu, Y.-H. Wu, and W. Hu, "Using wavelet transform and fuzzy neural network for vpc detection from the holter ecg," *IEEE Transactions on Biomedical Engineering*, vol. 51, no. 7, pp. 1269–1273, July 2004.
- [12] O. T. Inan, L. Giovangrandi, and G. T. A. Kovacs, "Robust neural-network-based classification of premature ventricular contractions using wavelet transform and timing interval features," *IEEE Transactions on Biomedical Engineering*, vol. 53, no. 12, pp. 2507–2515, December 2006.
- [13] F. Melgani and Y. Bazi, "Classification of electrocardiogram signals with support vector machines and particle swarm optimization," *IEEE Transactions on Information Technology in Biomedicine*, vol. 12, no. 5, pp. 667–677, September 2008.
- [14] D. A. Coast, R. M. Stern, G. G. Cano, and S. A. Briller, "An approach to cardiac arrhythmia analysis using hidden markov models," *IEEE Transactions on Biomedical Engineering*, vol. 37, no. 9, p. 826836, September 1990.
- [15] Y. H. Hu, S. Palreddy, and W. J. Tompkins, "A patient-adaptable ecg beat classifier using a mixture of experts approach," *IEEE Transactions on Biomedical Engineering*, vol. 44, no. 9, pp. 891–900, September 1997.
- [16] P. de Chazal and R. B. Reilly, "A patient-adapting heartbeat classifier using ecg morphology and heartbeat interval features," *IEEE Transactions on Biomedical Engineering*, vol. 53, no. 12, pp. 2535–2543, December 2006.
- [17] W. Jiang and S. G. Kong, "Block-based neural networks for personalized ecg signal classification," *IEEE Transactions on Neural Networks*, vol. 18, no. 6, pp. 1750–1761, November 2007.
- [18] T. Ince, S. Kiranyaz, and M. Gabbouj, "A generic and robust system for automated patient-specific classification of electrocardiogram signals," *IEEE Transactions on Biomedical Engineering*, vol. 56, no. 5, p. 14151426, May 2009.
- [19] R. Hoekema, G. J. H. Uijen, and A. van Oosterom, "Geometrical aspects of the interindividual variability of multilead ecg recordings," *IEEE Transactions on Biomedical Engineering*, vol. 48, no. 5, pp. 551–559, May 2001.
- [20] S. Kiranyaz, T. Ince, , and M. Gabbouj, "Real-time patient-specific ecg classification by 1-d convolutional neural networks," *IEEE Transactions on Biomedical Engineering*, vol. 63, no. 3, pp. 664–675, March 2016.
- [21] P. Rajpurkar, A. Y. Hannun, M. Haghighpanahi, C. Bourn, and A. Y. Ng, "Cardiologist-level arrhythmia detection with convolutional neural networks," *arXiv preprint arXiv: 1707.01836v1*, July 2017.
- [22] T. J. Jun, H. M. Nguyen, D. Kang, D. Kim, D. Kim, and Y.-H. Kim, "Ecg arrhythmia classification using a 2-d convolutional neural network," *arXiv preprint arXiv:1804.06812*, 2018.
- [23] P. Li, Y. Wang, J. He, L. Wang, Y. Tian, T. shu Zhou, T. Li, and J. song Li, "High-performance personalized heartbeat classification model for long-term ecg signal," *IEEE Transactions on Biomedical Engineering*, vol. 64, no. 1, pp. 78–86, Jan. 2017.
- [24] "How the heart works." [Online]. Available: <https://www.nhlbi.nih.gov/health-topics/how-heart-works>
- [25] *AAMI-recommended practice: Testing and reporting performance results of ventricular arrhythmia detection algorithms*. Arlington, VA: Association for the Advancement of Medical Instrumentation, 1987.
- [26] S. Chauhan and L. Vig, "Anomaly detection in ecg time signals via deep long short-term memory networks," in *Data Science and Advanced Analytics (DSAA), IEEE International Conference on*, December 2015.
- [27] A. Isin and S. Ozdalili, "Cardiac arrhythmia detection using deep learning," *Procedia Computer Science*, vol. 120, pp. 268–275, 2017.
- [28] F. yan Zhou, L. peng Jin, and J. Dong, "Premature ventricular contraction detection combining deep neural networks and rules inference," *Artificial Intelligence in Medicine*, 2017.
- [29] Ö. Yildirim, "A novel wavelet sequence based on deep bidirectional lstm network model for ecg signal classification," *Computers in biology and medicine*, vol. 96, pp. 189–202, 2018.
- [30] S. L. Oh, E. Y. Ng, R. San Tan, and U. R. Acharya, "Automated diagnosis of arrhythmia using combination of cnn and lstm techniques with variable length heart beats," *Computers in biology and medicine*, 2018.
- [31] B. A. Teplitzky and M. McRoberts, "Fully-automated ventricular ectopic beat classification for use with mobile cardiac telemetry," in *2018 IEEE 15th International Conference on Wearable and Implantable Body Sensor Networks (BSN)*, March 2018, pp. 58–61.
- [32] A. Page, A. Kulkarni, and T. Mohsenin, "Utilizing deep neural nets for an embedded ecg-based biometric authentication system," in *IEEE Biomedical Circuits and Systems Conference (BioCAS)*, 2015, pp. 1–4.
- [33] R. Salloum and C.-C. J. Kuo, "Ecg-based biometrics using recurrent neural networks," in *Acoustics, Speech and Signal Processing (ICASSP), IEEE International Conference on*, March 2017.
- [34] M. Zihlmann, D. Perekrestenko, and M. Tschannen, "Convolutional recurrent neural networks for electrocardiogram classification," *Computing*, vol. 44, p. 1, 2017.
- [35] P. Schwab, G. Scebba, J. Zhang, M. Delai, and W. Karlen, "Beat by beat: Classifying cardiac arrhythmias with recurrent neural networks," *CoRR*, vol. abs/1710.06319, 2017. [Online]. Available: <http://arxiv.org/abs/1710.06319>
- [36] E. D. Ubeyli, "Combining recurrent neural networks with eigenvector methods for classification of ecg beats," *Digital Signal Processing*, vol. 19, pp. 320 – 329, 2009.

- [37] —, “Recurrent neural networks employing lyapunov exponents for analysis of ecg signals,” *Expert Systems with Applications*, vol. 37, no. 2, pp. 1192 – 1197, March 2010.
- [38] B. Pourbabaei, M. J. Roshtkhari, and K. Khorasani, “Deep convolutional neural networks and learning ecg features for screening paroxysmal atrial fibrillation patients,” *IEEE Transactions on Systems, Man, and Cybernetics: Systems*, no. 99, pp. 1–10, 2017.
- [39] Y. Xia, N. Wulan, K. Wang, and H. Zhang, “Detecting atrial fibrillation by deep convolutional neural networks,” *Computers in biology and medicine*, vol. 93, pp. 84–92, 2018.
- [40] X. Fan *et al.*, “Multiscaled fusion of deep convolutional neural networks for screening atrial fibrillation from single lead short ecg recordings,” *IEEE Journal of Biomedical and Health Informatics*, vol. 22, no. 6, pp. 1744–1753, Nov 2018.
- [41] Z. C. Lipton, D. C. Kale, C. Elkan, and R. Wetzel, “Learning to diagnose with lstm recurrent neural networks,” *arXiv preprint arXiv: 1511.03677v7*, March 2017.
- [42] “Electrical conduction system of the heart.” [Online]. Available: en.wikipedia.org
- [43] R. G. Mark and G. B. Moody. (1997) MIT-BIH arrhythmia database. [Online]. Available: <http://ecg.mit.edu/dbinfo.html>
- [44] J. Pan and W. J. Tompkins, “A real-time qrs detection algorithm,” *IEEE Transactions on Biomedical Engineering*, vol. BME-32, pp. 230–236, May 1985.
- [45] H. Khamis, R. Weiss, Y. Xie, C. W. Chang, N. H. Lovell, and S. J. Redmond, “Qrs detection algorithm for telehealth electrocardiogram recordings,” *IEEE Transactions on Biomedical Engineering*, vol. 63, no. 7, pp. 1377 – 1388, July 2016.
- [46] S. G. Mallat, “A theory for multiresolution signal decomposition: The wavelet representation,” *IEEE Transactions on Pattern Analysis and Machine Intelligence*, vol. 11, no. 7, pp. 674 – 693, July 1989.
- [47] S. Hochreiter and J. Schmidhuber, “Long short-term memory,” *Neural Computation*, vol. 9, no. 8, pp. 1735–1780, November 1997.
- [48] F. A. Gers and J. Schmidhuber, “Recurrent nets that time and count,” in *Proceedings of the IEEE-INNS-ENNS International Joint Conference on Neural Networks (IJCNN)*, July 2000, pp. 189–194.
- [49] K. Cho, B. van Merriënboer, C. Gulcehre, F. Bougares, H. Schwenk, D. Bahdanau, and Y. Bengio, “Learning phrase representations using rnn encoder-decoder for statistical machine translation,” *arXiv preprint arXiv: 1406.1078*, 2014.
- [50] J. Sill, G. Takács, L. W. Mackey, and D. Lin, “Feature-weighted linear stacking,” *CoRR*, vol. abs/0911.0460, 2009. [Online]. Available: <http://arxiv.org/abs/0911.0460>
- [51] A. Toscher, M. Jahrer, and R. Bell. (2009, September) The bigchaos solution to the netflix grand prize. [Online]. Available: http://www.netflixprize.com/assets/GrandPrize2009_BPC_BigChaos.pdf
- [52] P. J. Werbos, “Generalization of backpropagation with application to a recurrent gas market model,” *Neural Networks*, vol. 1, no. 4, pp. 339 – 356, 1988.
- [53] D. P. Kingma and J. Ba, “Adam: a method for stochastic optimization,” in *International Conference on Learning Representations*, 2015, p. 113.
- [54] Y. Bengio, “Practical recommendations for gradient-based training of deep architectures,” *CoRR*, vol. abs/1206.5533, 2012. [Online]. Available: <http://arxiv.org/abs/1206.5533>